ACS Sustainable Chemistry & Engineering

Research Article

pubs.acs.org/journal/ascecg

Sustainable Catalysts from Gold-Loaded Polyamidoamine Dendrimer-Cellulose Nanocrystals

Li Chen,[†] Wuji Cao,[†] Patrick J. Quinlan,[†] Richard M. Berry,[‡] and Kam C. Tam*[,†]

[†]Department of Chemical Engineering, Waterloo Institute for Nanotechnology, University of Waterloo, 200 University Avenue W, Waterloo, Ontario N2L 3G1, Canada

[‡]CelluForce Inc., 625 Président-Kennedy Avenue, Montreal, Quebec H3A 1K2, Canada

Supporting Information

ABSTRACT: Generation 6.0 polyamidoamine (G6 PAMAM) dendrimer-grafted cellulose nanocrystals (CNCs) (CNC−PAMAM) were synthesized and employed as supports for gold nanoparticles. The successful grafting of PAMAM dendrimers was confirmed by conductometric−potentiometric titration and pH-dependent ζ-potential analyses. Gold nanoparticles with diameters of approximately 2 to 4 nm were synthesized with the PAMAM dendrimers playing the role of nanoreactors and $NaBH_4$ as the reducing agent. More importantly, gold nanoparticles were successfully prepared at pH 3.3 with the PAMAM dendrimers playing the functional role of reducing agent. Temperature and the concentration of CNC−PAMAM had an impact on the resulting size of gold nanoparticles. The gold nanoparticles immobilized on CNC−PAMAM displayed superior catalytic properties toward the reduction of 4-nitrophenol to 4-aminophenol. The enhanced catalytic behavior may be attributed to the improved dispersity and accessibility of gold nanoparticles within the PAMAM dendrimer domain. This work has demonstrated the versatility of CNC−PAMAM, both as an effective nanoreactor and a reducing agent.

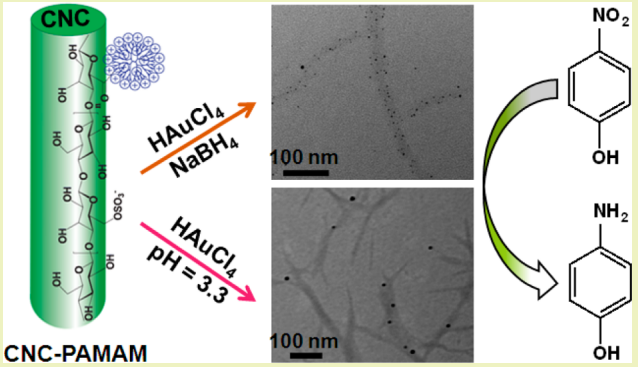

KEYWORDS: *Polyamidoamine dendrimer, Cellulose nanocrystals, Gold nanoparticle, Catalysts, Green synthesis, Particle size distribution*

INTRODUCTION

Gold nanoparticles have been employed in a myriad of applications, including bioimaging, biomedicine, chemical sensing and drug delivery.[1,2] They have also been explored as green catalysts for a variety of chemical reactions, including the oxidation of CO to CO_2, aerobic oxidation of alcohols, C−C coupling reactions and reduction reactions via transfer hydrogenation.[3] As was observed with other nanoparticle catalysts, gold nanoparticles have a propensity to aggregate in solution, which hinders their performance and ultimately limits their application. In an effort to stabilize gold nanoparticles in solution, complexation with a range of compounds including, but not limited to, thiols, carboxylate ligands, surfactants and polyelectrolytes have been investigated.[4] However, many of these stabilizers are hampered by their low stability, potential toxicity, poor biocompatibility or limited biodegradability.[5] Another method in preventing aggregation is the homogeneous deposition of gold nanoparticles onto a template material, such as graphene sheets,[6] carbon nanotubes,[7] TiO_2[8] and SiO_2 spheres.[9] However, most of the template materials explored thus far lack sufficient functional groups with a metal affinity, such as $-NH_2$, −SiH and −SH, to effectively stabilize and disperse gold nanoparticles.[10]

Recently, cellulose nanocrystals have been explored as renewable biotemplates due to their shape, stability in aqueous solution, good mechanical strength, high specific surface area, biocompatibility and biodegradability.[11] These attractive features make cellulose nanocrystals (CNCs) promising supports for inorganic nanoparticles, such as Au,[12,13] Ag,[14] Ag−Au alloy,[15] Pd,[16,17] Pt,[18] Se[19] and Fe_3O_4.[20,21] However, generating uniformly dispersed nanoparticle-containing CNCs with well-controlled size and structure remains a challenge. Moreover, the electrostatic attraction that exists between metal ions in solution and sulfate ester moieties present on the surface of CNCs can induce severe irreversible aggregation and phase separation.[15] Since aggregation makes the catalyst surface less accessible to reactants, it reduces the performance of the catalytic system. To circumvent these undesirable characteristics, it is necessary to modify the CNC surface with metal-affinity groups and develop new strategies to minimize particle aggregation.

In this study, poly(amidoamine) (PAMAM) dendrimers were covalently grafted onto the surface of oxidized CNCs (CNC−COOH) via amide bonds. PAMAM dendrimers have a well-

Received: February 11, 2015
Revised: March 31, 2015
Published: April 13, 2015

DOI: 10.1021/acssuschemeng.5b00110
ACS Sustainable Chem. Eng. 2015, 3, 978−985

defined three-dimensional hyper-branched structure, with primary and tertiary amine groups present at the dendrimer surface and core, respectively. The dissociation properties of these two types of amine groups impart attractive pH-responsive structural changes to the dendrimer.[22,23] Under acidic conditions in aqueous media, the cavities within the PAMAM dendrimers are ideal nanoreactors for producing and hosting inorganic nanoparticles, such as Au,[24,25] Ag,[26] Pt[27] and Pd.[28] The well-defined structure and size of the cavities yield a narrow size distribution for loaded nanoparticles and the electrostatic and steric repulsions minimize aggregation of the nanoparticles. In contrast to capping agents, each inorganic nanoparticle is stabilized by one dendrimer, imparting high structural stability. The surface of these inorganic nanoparticles is often unpassivated and fully accessible during the catalytic process,[29] which enhances the catalytic performance.[30]

Compounds with abundant amino groups have been applied as metal binding groups,[31] stabilizers[32] and reducing agents[33] for the preparation of inorganic nanoparticles. Their ability to reduce metal ions facilitates the synthesis of inorganic nanoparticles via a simple and green synthetic process. In this work, a CNC−PAMAM hybrid, with abundant metal-binding NH_2 groups, was used as a support and reducing agent for gold nanoparticles. Gold nanoparticles were prepared using sodium borohydride and PAMAM dendrimers as reducing agents. The effects of CNC−PAMAM concentration and temperature on the size of the resulting gold nanoparticles were studied. All CNC−PAMAM−Au systems were stable and dispersible in acidic solution. The catalytic activity of the two systems was evaluated by the reduction of 4-nitrophenol (4-NP) to 4-aminophenol (4-AP). An added benefit of complexing gold nanoparticles with CNC−PAMAM is that it allowed for direct observation of the complex under transmission electron microscopy (TEM), which can also be used to confirm the successful grafting of the PAMAM dendrimer on the CNC surface. Finally, the pH-responsive property of CNC−PAMAM may simplify the separation process and the recycling of the catalysts.

EXPERIMENTAL SECTION

Materials. Generation 6.0 poly(amidoamine) dendrimers (G6 PAMAM, 5% w/w solution in methanol), sodium hypochlorite (NaClO, 10−15% available chlorine), *N*-hydroxysuccinimide (NHS, 98%), sodium bromide (NaBr, ≥99.0%), gold(III) chloride trihydrate ($HAuCl_4$, ≥99.9%), 2-(*N*-morpholino)ethanesulfonic acid hydrate (MES buffer, ≥99.5%), *N*-(3-(dimethylamino)propyl)-*N*′-ethylcarbodiimide hydrochloride (EDC, ≥98.0% AT), sodium borohydride ($NaBH_4$, ≥98.0%) and 4-nitrophenol (4-NP, ≥99.5%) were purchased from Sigma-Aldrich and used without further modification. CNCs were supplied by CelluForce, Inc. Purified water was obtained from a Millipore Milli-Q water purification system and was used in preparing all sample solutions.

Methods. *TEMPO Mediated Oxidation of CNCs.* Oxidized CNCs (CNC−COOH) were prepared according to the method described in a previous report.[34] Typically, 5 g of CNCs was dispersed in 375 mL of water under sonication. A 10 mL aqueous solution containing 0.0125 g of TEMPO and 0.125 g of NaBr was then added, followed by the addition of 50 mL of NaClO (10−15% w/w). Upon the introduction of NaClO, the dispersion became cloudy, and light yellowish. Sodium hydroxide (0.1 M) was used to maintain a pH value of 10.5 throughout the reaction. After the solution had reacted for 4 h, 5 mL of ethanol was added to terminate the oxidation and hydrochloride acid (0.1 M) was used to adjust the pH to 7. The reaction product was purified by dialysis and freeze-dried.

G6 PAMAM Grafting onto CNCs. The carbodiimide-mediated amidation reaction[35] was used for grafting. CNC−PAMAM was prepared using a previous published procedure.[36] 50 mg of CNC−COOH was dispersed into MES buffer (pH 6.5, 25 mM) with sonication. Then, 100 mg of EDC and 100 mg of NHS were introduced into the dispersion, and the mixture was sonicated for 10 min, followed by stirring for 2 h. Next, the mixture was added dropwise to a flask containing 500 μL of 5% w/w G6 PAMAM dendrimer in 10 mL of water. The reaction was stirred for 24 h, and the CNC−PAMAM product was purified by dialysis and ultrafiltration.

Scheme 1. Schematic Illustration of the CNC−PAMAM−Au Synthetic Process[a]

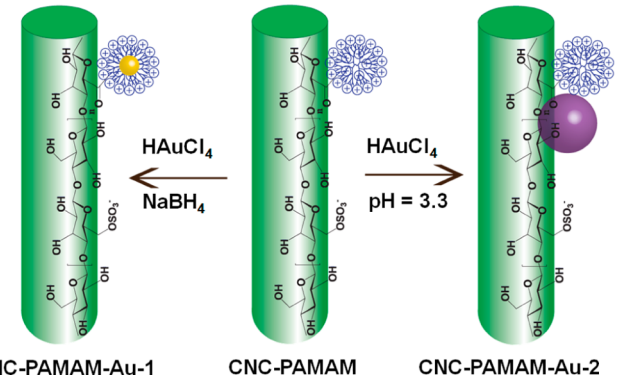

[a]The blue spheres represent PAMAM dendrimers, whereas the yellow and purple spheres signify small and large gold nanoparticles, respectively.

Synthesis of CNC−PAMAM−Au-1 (Scheme 1). The pH of a 10 mL 0.008% w/w CNC−PAMAM solution was adjusted to 3.3, and the solution was stirred for 30 min. 100 μL of 5 mM $HAuCl_4$ was then added, and the mixture was stirred for 1 h to allow for the adsorption of $AuCl_4^-$ onto CNC−PAMAM. 100 μL of 0.05 M $NaBH_4$ was added under vigorous stirring, and the initially colorless solution immediately became light brown. The reaction was continued for another 20 min and purified by dialysis.

Synthesis of CNC−PAMAM−Au Using CNC−PAMAM as Reducing Agents (Scheme 1). 100 μL of 5 mM $HAuCl_4$ was added to 10 mL CNC−PAMAM aqueous solutions of varying concentrations. The mixtures were stirred for a designated period of time at a given temperature. By the end of the reactions, the initially colorless solutions had turned red. Details on the synthesis of CNC−PAMAM−Au nanohybrids are summarized in Table 1.

Evaluation of Catalytic Performance. A 2.5 mL solution containing 0.10 mM 4-NP and 40 mM $NaBH_4$ was prepared. Then 50 μL of 0.009% w/w CNC−PAMAM−Au (Au content: 2.5 nmol) was added to the mixture. The reaction was carried out at room temperature in a quartz cuvette and monitored via UV−vis spectrophotometry.

Characterization. The morphologies of CNCs, CNC−COOH, CNC−PAMAM and CNC−PAMAM−Au were evaluated using a Philip CM 10 transmission electron microscope under an accelerating voltage of 60 kV. TEM samples were prepared by spraying 10 μL of a 0.01% w/w dispersion onto a carbon-coated copper grid and dried. The concentrations of functional groups were determined through conductometric-potentiometric titration using a Metrohm 809 Titrando autotitrator. The ζ-potential and size distribution of CNCs, CNC−COOH and the CNC−PAMAM system were measured using a Malvern Nano-ZS90 Zetasizer. The pH values of the solutions were adjusted using the autotitrator. Titrant solutions (0.1 M HCl or 0.1 M NaOH) were introduced at a flow rate of 0.1 mL/min. Successive UV−vis absorption spectra were obtained using a Shimadzu U-3000 spectrophotometer with a specified scanning interval of 1 min.

DOI: 10.1021/acssuschemeng.5b00110
ACS Sustainable Chem. Eng. 2015, 3, 978−985

Table 1. Summary of Synthetic Conditions for Preparing CNC−PAMAM−Au System

nanohybrids	CNC−PAMAM (w/w %)	$HAuCl_4$ (5 mM) (μL)	reducing agent	T (°C)	time (h)
CNC−PAMAM−Au-1	0.008	100	$NaBH_4$	25	2
CNC−PAMAM−Au-2	0.040	100	CNC−PAMAM	25	24
CNC−PAMAM−Au-3	0.020	100	CNC−PAMAM	25	24
CNC−PAMAM−Au-4	0.008	100	CNC−PAMAM	25	24
CNC−PAMAM−Au-5	0.008	100	CNC−PAMAM	50	1
CNC−PAMAM−Au-6	0.008	100	CNC−PAMAM	75	0.5

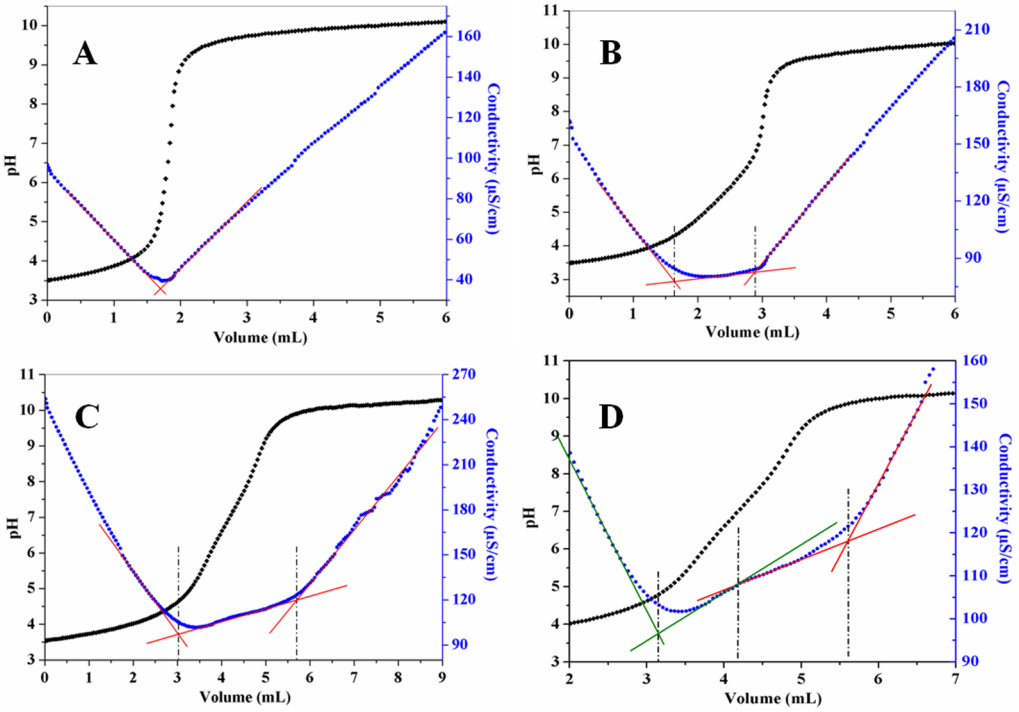

Figure 1. Simultaneous conductometric−potentiometric titration curves of 0.03% w/w CNCs (A), CNC−COOH (B), CNC−PAMAM (C and D).

RESULTS AND DISCUSSION

Conductometric−potentiometric titration has been widely applied to determine the amount of weak acid in cellulose-based systems.[37,38] In a typical procedure, a 0.03% w/w sample dispersion was prepared and the pH was adjusted to ~3 by adding 0.1 M HCl, followed by titration using 0.01 M NaOH and simultaneous measurements of solution conductivity and pH. The concentrations of specific functional groups were determined from the quantity of NaOH required to reach the equivalence points. The titration curve of CNCs is shown in Figure 1A. One equivalence point (EP), attributed to the neutralization of excess H^+ from HCl, was observed. In Figure 1B, the titration curve of CNC−COOH exhibits two EPs, with the first indicating the neutralization of free H^+ and the second signifying the complete dissociation of carboxyl groups. The three regions from left to right correspond to strong acid neutralization, weak acid neutralization and the addition of excess base. From the amounts of NaOH titrated in the second stage, the carboxylate content on CNC−COOH was calculated to be approximately 1.05 mmol/g. Figure 1C,D display the three EPs observed for CNC−PAMAM. The second and third EPs indicate the complete dissociation of carboxyl and amino groups, respectively. The carboxyl and amino content were evaluated to be approximately 0.85 and 1.20 mmol/g, respectively. The titration details are summarized in Table 2.

Table 2. Calculated Concentrations of Carboxyl and Amine Groups on CNCs, CNC−COOH and CNC−PAMAM

sample	carboxyl groups (mmol/g)	amino groups (mmol/g)
CNCs	0	0
CNC−COOH	1.05	0
CNC−PAMAM	0.85	1.20

The ζ-potential is commonly used to measure the electrostatic potential of nanoparticles at the electrical double layer. Because both CNC−COOHs and PAMAM dendrimers possess pH-dependent functional groups, it is important to analyze and understand the effect of pH on the surface charge of CNC−PAMAM. The pH-dependent ζ-potential of CNC−PAMAM is shown in Figure 2A. At pH 3, the surface of CNC−PAMAM was highly cationic, with a ζ-potential value of +52 mV. The observed positive charge is a result of the protonation of amine groups on the surface grafted PAMAM dendrimers. Increasing the pH resulted in a reduction in the ζ-potential of CNC−PAMAM due to the deprotonation of carboxyl groups present on the CNC surface. The highly positive ζ-potential values observed for pH $\leq$ 7 suggest a high PAMAM grafting density. Further increase in the pH resulted in the complete deprotonation of amino groups, as illustrated by the corresponding reduction in ζ-potential. This resulted in particle instability and formation of precipitates, as depicted in Figure 2B. As the pH approached 10, the ζ-potential

DOI: 10.1021/acssuschemeng.5b00110
ACS Sustainable Chem. Eng. 2015, 3, 978−985

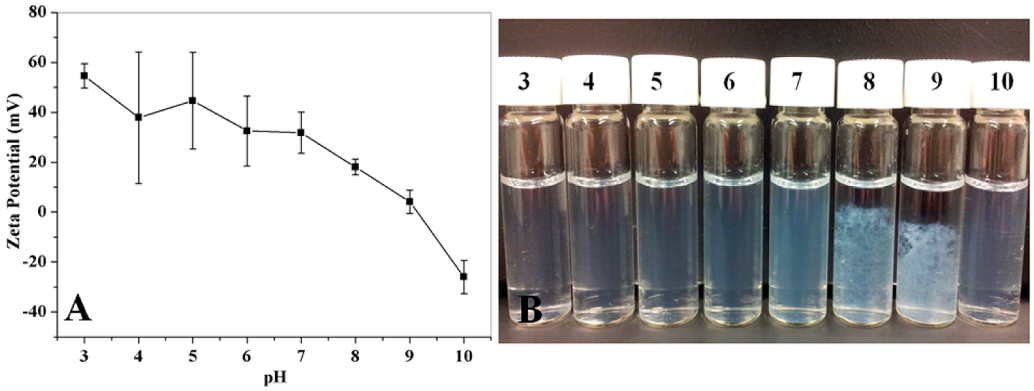

Figure 2. pH-dependent ζ-potential (A) and corresponding optical photographs (B) of 0.08% w/w CNC−PAMAM solutions.

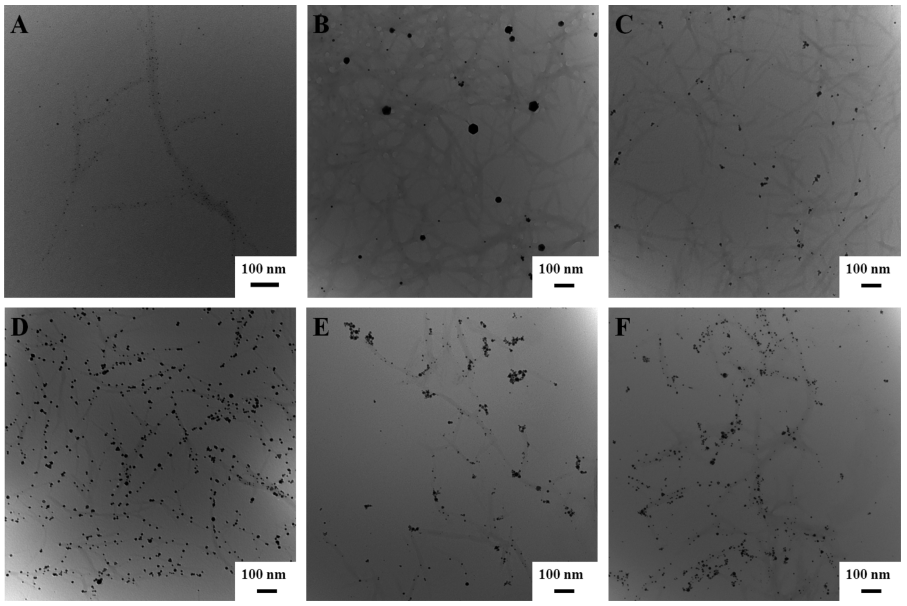

Figure 3. TEM images of CNC−PAMAM−Au-1 (A), CNC−PAMAM−Au-2 (B), CNC−PAMAM−Au-3 (C), CNC−PAMAM−Au-4 (D), CNC−PAMAM−Au-5 (E, and CNC−PAMAM−Au-6 (F).

of CNC−PAMAM decreased to −30 mV due to the exposure of unreacted carboxylate and sulfate ester groups on the CNC surface. The pH dependent behavior of CNC−PAMAM offers chemical and physical properties that may be valuable for applications ranging from pharmaceutical delivery to Pickering emulsification.

Dynamic light scattering (DLS) was used to measure the size distributions of CNCs, CNC−COOH and CNC−PAMAM (Figure S1 of the Supporting Information). CNC−COOH was slightly smaller than the unmodified CNC, which may be attributed to the improved dispersity of CNC−COOH and the slight degradation of CNC during the alkaline oxidation process. PAMAM grafting on the surface of CNC−COOH, however, yielded particles 2 times the size of unmodified CNC, as well as a small number of aggregates with a size of 1 to 2 μm. The presence of micron-sized particles suggested the existence of CNC cross-linking via the amine groups present on the PAMAM dendrimers. To further investigate the presence of cross-linking and the overall morphology of the particles, TEM images were taken for both CNC−COOH (Figure S2A of the Supporting Information) and CNC−PAMAM (Figure S2B of the Supporting Information). Figure S2A of the Supporting Information shows well-dispersed CNC−COOH particles, with lengths ranging from 200 to 400 nm. Meanwhile, nanorod bundles are observed in Figure S2B of the Supporting Information, confirming the hypothesis that some cross-linking exists between CNC−PAMAM particles. Although cross-linking could not be completely avoided during the synthesis process, the PAMAM grafting reaction was still well controlled, and stable dispersions of CNC−PAMAM in water were achievable under acidic and alkaline conditions (Figure 2B).

Due to their small size, it is often difficult to observe dendrimers under TEM. One way to facilitate the direct observation is to encapsulate metal particles within the dendrimer network.[39] In this study, gold nanoparticles were not only used to provide additional functionality to CNC−PAMAM, but also to confirm the successful grafting of PAMAM on CNC. CNC−PAMAM−Au-1 was prepared using $NaBH_4$ as the reducing agent (Table 1). Figure 3A shows the well-dispersed gold nanoparticles on the order of 2 to 4 nm on CNC−PAMAM, which confirmed the successful grafting of PAMAM dendrimers on CNC.

In a recent study, it was suggested that polymers rich in amine functionality may serve as effective reducing agents for the synthesis of gold nanoparticles.[33] To investigate the efficacy of CNC−PAMAM as both a nanoreactor and reducing agent, gold

DOI: 10.1021/acssuschemeng.5b00110
ACS Sustainable Chem. Eng. 2015, 3, 978−985

nanoparticles were prepared on the surface of CNC−PAMAM in the absence of $NaBH_4$ over a range of pH values. Figure 4 shows

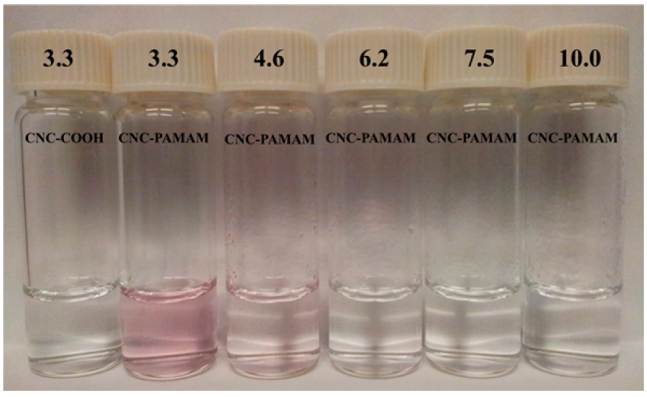

Figure 4. Optical photograph of CNC−COOH and CNC−PAMAM solutions after the introduction of $AuCl_4^-$.

the successful reduction of $AuCl_4^-$ by CNC−PAMAM (0.008% w/w) under mild acidic conditions (pH 3.3 and 4.6). The production of gold nanoparticles caused the solution to turn into a red dispersion. No color change was observed under neutral and basic conditions (pH ≥ 6.2), indicating that the protonated amine groups played an important role in the reduction of $AuCl_4^-$ to Au^0. Large CNC−PAMAM aggregates were observed for pH ≥ 4.6 due to electrostatic attraction between protonated amine groups and $AuCl_4^-$. However, the sufficiently high positive surface charge of CNC−PAMAM at pH 3.3 allowed for the solution to remain stable. Therefore, all subsequent synthetic reactions were maintained at pH 3.3.

To study the effect of CNC−PAMAM concentration on the size of the resulting gold nanoparticles, three concentrations (0.040%, 0.020% and 0.008% w/w) were used for the reduction of $HAuCl_4$ at 25 °C. TEM images were obtained to elucidate the morphologies of the resulting CNC−PAMAM hybrids (CNC−PAMAM−Au-2, CNC−PAMAM−Au-3 and CNC−PAMAM−Au-4, respectively). The TEM image of CNC−PAMAM−Au-2 showed gold nanoparticles with diameters in the range of approximately 10 to 50 nm (Figure 3B). Meanwhile, the TEM images of CNC−PAMAM−Au-3 (Figure 3C) and CNC−PAMAM−Au-4 (Figure 3D) displayed gold nanoparticles with diameters of less than 20 nm. Further, the particle size distributions became more uniform when the concentration of CNC−PAMAM was reduced. These results indicated that a high concentration of CNC−PAMAM resulted in a rapid $HAuCl_4$ reduction and nanoparticle growth, yielding a broad size distribution of gold nanoparticles bound to CNC−PAMAM. Therefore, better control of the gold nanoparticle size and distribution could be achieved using a lower CNC−PAMAM concentration.

To evaluate the effect of temperature on the size of gold nanoparticles, CNC−PAMAM (0.008% w/w) was also used to reduce $HAuCl_4$ at 50 °C for 1 h (CNC−PAMAM−Au-5) and 75 °C for 0.5 h (CNC−PAMAM−Au-6). The reaction time was significantly shortened due to the increased reaction rate at higher temperatures. Using a low CNC−PAMAM concentration (0.008% w/w), no large gold nanoparticles were observed. However, minor aggregation of the particles was evident, which broadened the overall particle size distributions. Upon comparing CNC−PAMAM−Au-5 (Figure 3E) with CNC−PAMAM−Au-6 (Figure 3F), we observed the latter displayed a slight increase in the size of the particles, which may have resulted from the rapid reduction and particle growth rate at the elevated temperature.

The effects of concentration and temperature on gold nanoparticle size were further confirmed by TEM images of CNC−PAMAM−Au nanohybrids synthesized with different concentrations of CNC−PAMAM at 75 °C. The TEM images revealed the presence of larger aggregates and increased size of gold nanoparticles with 0.040% and 0.020% CNC−PAMAM (Figure S3 of the Supporting Information). Therefore, good dispersion and narrow size distribution of gold nanoparticles are more likely to be achieved at moderate temperature in low concentration of CNC−PAMAM, with PAMAM serving as the reducing agent. However, particle-size distributions are much narrower for products obtained using $NaBH_4$ as the reducing agent. Generally, no large CNC−PAMAM aggregates were observed for all products, and the attachment of gold nanoparticles on the CNC surfaces were evident, confirming the successful grafting of G6 PAMAM dendrimers on CNCs. With the abundant positive surface charges at pH 3.3, all CNC−PAMAM−Au hybrid systems were very stable, with no observable precipitates forming within a 1 month period.

UV−vis absorption spectra of CNC−PAMAM−Au nanohybrids were measured from 300 to 700 nm (Figure 5). These

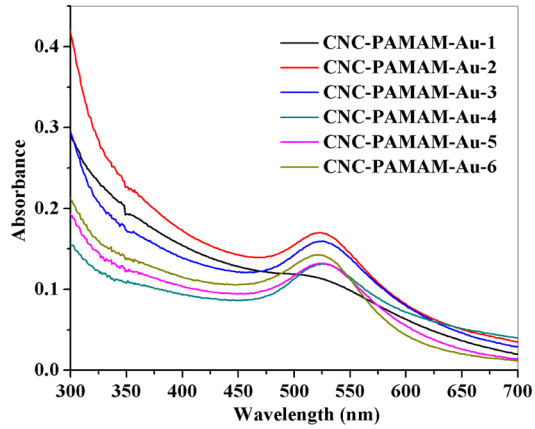

Figure 5. UV−vis absorption spectra of CNC−PAMAM−Au nanohybrids.

absorption peaks result from localized surface plasmon oscillation and are characteristics of small gold nanoparticles.[40] CNC−PAMAM−Au-1 possessed a light pinkish color and a weak, broad absorption peak centered at approximately 510 nm. The CNC−PAMAM−Au nanohybrids produced in the absence of $NaBH_4$, on the other hand, exhibited a rich red wine color and a strong absorption peak at approximately 525 nm. Compared with CNC−PAMAM−Au-1, the observed red shift suggests an increase in the size of the gold nanoparticles, which agrees with the TEM micrographs.

To evaluate the catalytic activity of gold nanoparticles loaded on CNC−PAMAM, the reduction of 4-NP to 4-AP in the presence of excess $NaBH_4$ and CNC−PAMAM−Au was tested. The corresponding rates of reaction were calculated using the pseudo-first-order kinetic model, where the reduction process was monitored by UV−vis spectrophotometry. Figure S4 of the Supporting Information shows that, in the absence of a catalyst, no reduction of 4-NP occurred. However, when CNC−PAMAM−Au was introduced to the system, the absorbance peak ascribed to 4-NP at 400 nm decreased as a function of time,

DOI: 10.1021/acssuschemeng.5b00110
ACS Sustainable Chem. Eng. 2015, 3, 978−985

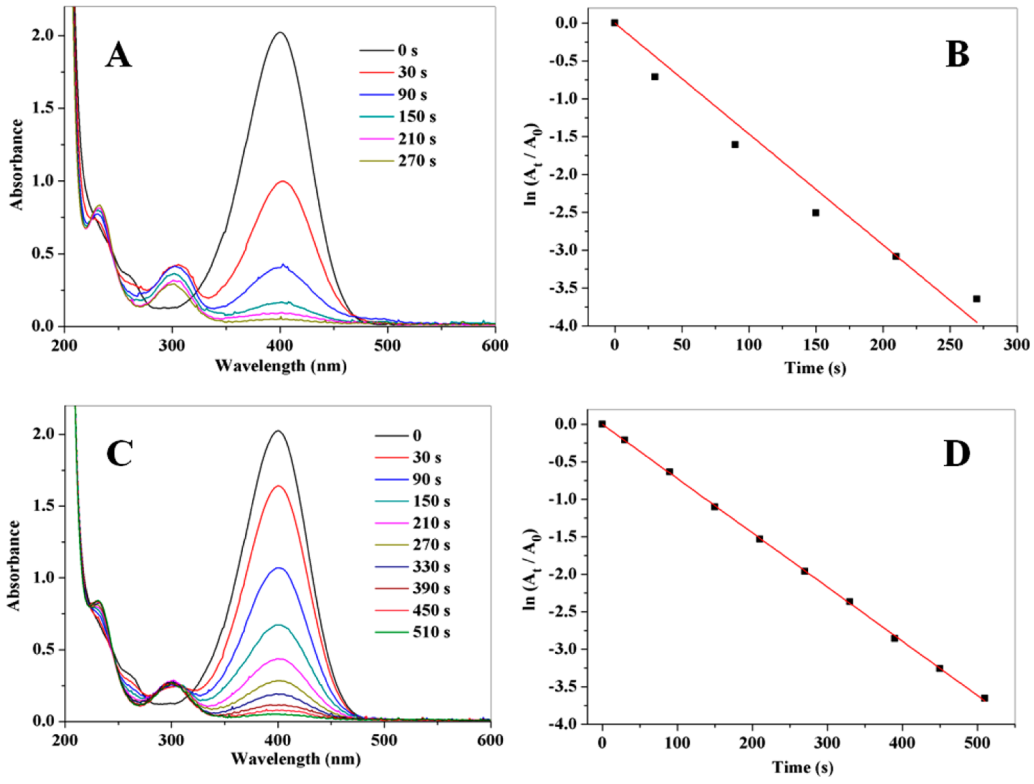

Figure 6. Successive UV−vis absorption spectra of the reduction of 4-NP by $NaBH_4$ in the presence of CNC−PAMAM−Au-1 (A) and CNC−PAMAM−Au-4 (C); corresponding logarithm of the absorbance at 400 nm as a function of time (B and D).

Table 3. Catalytic Performance of Six CNC−PAMAM−Au Systems

sample	Au nanoparticle diameter (nm)	pseudo-first-order rate constant k (s^{-1})	activity factor κ (s^{-1} g^{-1})	turnover frequency TOF (h^{-1})
CNC−PAMAM−Au-1	2−4	0.015	3333	5400
CNC−PAMAM−Au-2	10−50	2.2×10^{-3}	489	792
CNC−PAMAM−Au-3	10−20	4.5×10^{-3}	1000	1620
CNC−PAMAM−Au-4	10−20	7.2×10^{-3}	1600	2590
CNC−PAMAM−Au-5	10−25	6.7×10^{-3}	1489	2410
CNC−PAMAM−Au-6	10−25	5.1×10^{-3}	1133	1840

while a new peak assigned to 4-AP at 290 nm appeared. The catalytic reduction was complete within 270 s for CNC−PAMAM−Au-1 (Figure 6A) and 510 s for CNC−PAMAM−Au-4 (Figure 6C). Linear correlations between $\ln(A_t/A_0)$ (A_t and A_0 represent the absorbance values of 4-NP at 400 nm at designated time t and t = 0, respectively) and the kinetic parameters were obtained (Figure 6B,D). The pseudo-first-order rate constant k was 1.5×10^{-2} and 7.2×10^{-3} s^{-1} for CNC−PAMAM−Au-1 and CNC−PAMAM−Au-4, respectively. These results indicated that the smaller gold nanoparticles present on the surface of CNC−PAMAM−Au-1 displayed a more efficient catalytic performance. The improved efficiency is attributed to their larger specific surface area, which provided more accessible area for the reduction reaction to occur.[41] The activity factor κ, which is a ratio of the rate constant k over the total catalyst mass, was calculated in order to compare the present results with those of previously reported studies. κ was estimated to be 3333 and 1600 s^{-1} g^{-1} for CNC−PAMAM−Au-1 and CNC−PAMAM−Au-4, respectively. In comparison with a recently reported Au/graphene catalyst (κ = 31.7 s^{-1} g^{-1}),[42] the environmentally friendly and sustainable catalysts described here offer 2 orders of magnitude improvement. The turnover frequency (TOF), which represents the number of moles of 4-NP reacted per mole Au per hour, was evaluated for each system and found to be 5400 and 2590 h^{-1}.

The catalytic performances of various CNC−PAMAM−Au nanohybrids were evaluated under similar conditions, and the results are summarized in Table 3. The successive UV−vis absorption spectra and the corresponding logarithm of the absorbance at 400 nm as a function of time are shown in Figure S5 of the Supporting Information for CNC−PAMAM−Au-2 and CNC−PAMAM−Au-3 (effect of CNC−PAMAM concentration) and Figure S6 of the Supporting Information for CNC−PAMAM−Au-5 and CNC−PAMAM−Au-6 (effect of temperature). The results show that CNC−PAMAM−Au-2 exhibited the lowest catalytic activity, likely a result of the larger gold nanoparticles. Other products using CNC−PAMAM dendrimers as the reducing agent for gold nanoparticles displayed good catalytic behavior. No significant trends were observed in their catalytic performance. In general, these results confirmed the relatively high catalytic efficiency of the CNC−PAMAM−Au systems, which may be attributed to accessible, well-dispersed, and unpassivated gold nanoparticles present on CNC−PAMAM.

It is often valuable to recover and reuse noble metal nanoparticle catalysts. By taking advantage of the pH-responsive characteristics of these new nanostructure systems, the catalysts

DOI: 10.1021/acssuschemeng.5b00110
ACS Sustainable Chem. Eng. 2015, 3, 978−985

could be readily recovered by adjusting the pH to neutral, inducing particle aggregation. The aggregated nanocatalysts could then be recovered via filtration, washed and recycled for at least three cycles (Figure 7). This recyclability of the CNC−PAMAM−Au is particularly relevant its application in large-scale operations.

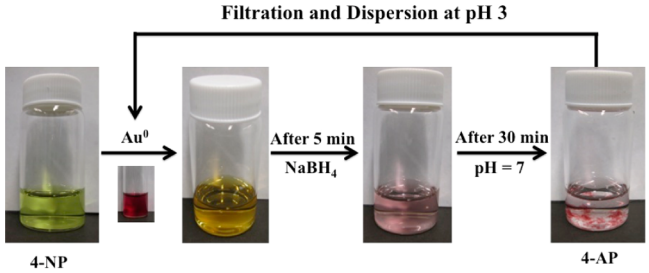

Figure 7. Schematic illustration demonstrating the recyclability of the CNC−PAMAM−Au catalytic process.

CONCLUSIONS

PAMAM dendrimers were successfully grafted onto oxidized CNCs using carbodiimide-mediated amidation reaction. Fourier transform infrared (FTIR) and pH-dependent ζ-potential values confirmed the presence of PAMAM dendrimers on the CNC surface. The size of the CNC−PAMAM hybrid, as determined by DLS, was greater than that of CNC and CNC−COOH. The TEM image of CNC−PAMAM showed that the characteristic rod-like CNC structure was preserved, confirming that the grafting reaction was well controlled. Gold nanoparticles of different sizes were formed on the CNC−PAMAM hybrid using $NaBH_4$ or PAMAM dendrimers as reducing agents. The use of $NaBH_4$ resulted in homogeneously dispersed gold nanoparticles (CNC−PAMAM−Au-1) with sizes in the range of 2−4 nm in diameter. The size distributions of gold nanoparticles were much broader for products obtained using PAMAM dendrimers as the reducing agents. The effects of CNC−PAMAM concentration and temperature on gold nanoparticle size were investigated. No significant difference was observed for their catalytic activities, with the exception of CNC−PAMAM−Au-2, which exhibited the lowest catalytic activity due to the large size and low specific surface area of the bound gold nanoparticles. CNC−PAMAM−Au-1 and CNC−PAMAM−Au-4 systems displayed good catalytic properties toward reducing 4-NP to 4-AP, with rate constants of 1.5×10^{-2} and 7.2×10^{-3} s^{-1}, respectively. In addition, simple separation and recovery was achieved by adjusting the pH of the system, causing the catalyst particles to phase separate from the solution. Based on the well-studied encapsulation of inorganic nanoparticles within PAMAM dendrimers, other functional inorganic nanoparticle complexes can be further explored.

ASSOCIATED CONTENT

Supporting Information

Size distributions of CNCs and CNC−COOH at pH 6.5 and CNC−PAMAM at pH 3.5, TEM images of CNC−COOH, CNC−PAMAM and CNC−PAMAM−Au nanohybrids synthesized at 75 °C; successive UV−vis absorption spectra of the reduction of 4-nitrophenol by $NaBH_4$ in the absence of catalysts; figures demonstrating the catalytic performance of CNC−PAMAM−Au-2, CNC−PAMAM−Au-3, CNC−PAMAM−Au-5 and CNC−PAMAM−Au-6. This material is available free of charge via the Internet at http://pubs.acs.org.

AUTHOR INFORMATION

Corresponding Author

*K. C. Tam. Tel.: 519-888-4567, ext. 38339. Fax: 519-888-4347. E-mail: mkctam@uwaterloo.ca.

Notes

The authors declare no competing financial interest.

ACKNOWLEDGMENTS

We acknowledge Celluforce Inc. for supplying the CNC used in this study. Research funding from CelluForce and AboraNano facilitated the research involving CNCs. K. C. Tam acknowledges funding from CFI and NSERC. We acknowledge Jingyi Liu for her assistance in schematic illustrations.

REFERENCES

(1) Saha, K.; Agasti, S. S.; Kim, C.; Li, X.; Rotello, V. M. Gold nanoparticles in chemical and biological sensing. *Chem. Rev.* **2012**, *112*, 2739−2779.

(2) Dreaden, E. C.; Alkilany, A. M.; Huang, X.; Murphy, C. J.; El-Sayed, M. A. The golden age: Gold nanoparticles for biomedicine. *Chem. Soc. Rev.* **2012**, *41*, 2740−2779.

(3) Stratakis, M.; Garcia, H. Catalysis by supported gold nanoparticles: Beyond aerobic oxidative processes. *Chem. Rev.* **2012**, *112*, 4469−4506.

(4) Daniel, M. C.; Astruc, D. Gold nanoparticles: Assembly, supramolecular chemistry, quantum-size-related properties, and applications toward biology, catalysis, and nanotechnology. *Chem. Rev.* **2004**, *104*, 293−346.

(5) Shi, Z.; Tang, J.; Chen, L.; Yan, C.; Tanvir, S.; Anderson, W. A.; Berry, R. M.; Tam, K. C. Enhanced colloidal stability and antibacterial performance of silver nanoparticles/cellulose nanocrystal hybrids. *J. Mater. Chem. B* **2015**, *3*, 603−611.

(6) Muszynski, R.; Seger, B.; Kamat, P. V. Decorating graphene sheets with gold nanoparticles. *J. Phys. Chem. C* **2008**, *112*, 5263−5266.

(7) Jiang, K.; Eitan, A.; Schadler, L. S.; Ajayan, P. M.; Siegel, R. W.; Grobert, N.; Mayne, M.; Reyes-Reyes, M.; Terrones, H.; Terrones, M. Selective attachment of gold nanoparticles to nitrogen-doped carbon nanotubes. *Nano Lett.* **2003**, *3*, 275−277.

(8) Zanella, R.; Giorgio, S.; Henry, C. R.; Louis, C. Alternative methods for the preparation of gold nanoparticles supported on TiO_2. *J. Phys. Chem. B* **2002**, *106*, 7634−7642.

(9) Pol, V. G.; Gedanken, A.; Calderon-Moreno, J. Deposition of gold nanoparticles on silica spheres: A sonochemical approach. *Chem. Mater.* **2003**, *15*, 1111−1118.

(10) Dong, F.; Guo, W.; Park, S. K.; Ha, C. S. Controlled synthesis of novel cyanopropyl polysilsesquioxane hollow spheres loaded with highly dispersed Au nanoparticles for catalytic applications. *Chem. Commun.* **2012**, *48*, 1108−1110.

(11) Lam, E.; Male, K. B.; Chong, J. H.; Leung, A. C. W.; Luong, J. H. T. Applications of functionalized and nanoparticle-modified nanocrystalline cellulose. *Trends Biotechnol.* **2012**, *30*, 283−290.

(12) Wu, X.; Lu, C.; Zhou, Z.; Yuan, G.; Xiong, R.; Zhang, X. Green synthesis and formation mechanism of cellulose nanocrystal-supported gold nanoparticles with enhanced catalytic performance. *Environ. Sci.: Nano.* **2014**, *1*, 71−79.

(13) John, H. T. Catalysis using gold nanoparticles decorated on nanocrystalline cellulose. *Nanoscale* **2012**, *4*, 997−1002.

(14) Drogat, N.; Granet, R.; Sol, V.; Memmi, A.; Saad, N.; Koerkamp, C. K.; Bressollier, P.; Krausz, P. Antimicrobial silver nanoparticles generated on cellulose nanocrystals. *J. Nanopart. Res.* **2011**, *13*, 1557−1562.

(15) Shin, Y.; Bae, I.-T.; Arey, B. W.; Exarhos, G. J. Facile stabilization of gold-silver alloy nanoparticles on cellulose nanocrystal. *J. Phys. Chem. C* **2008**, *112*, 4844−4848.

DOI: 10.1021/acssuschemeng.5b00110
ACS Sustainable Chem. Eng. 2015, 3, 978−985

(16) Cirtiu, C. M.; Dunlop-Brière, A. F.; Moores, A. Cellulose nanocrystallites as an efficient support for nanoparticles of palladium: Application for catalytic hydrogenation and Heck coupling under mild conditions. *Green Chem.* **2011**, *13*, 288−291.
(17) Rezayat, M.; Blundell, R. K.; Camp, J. E.; Walsh, D. A.; Thielemans, W. Green one-step synthesis of catalytically active palladium nanoparticles supported on cellulose nanocrystals. *ACS Sustainable Chem. Eng.* **2014**, *2*, 1241−1250.
(18) Johnson, L.; Thielemans, W.; Walsh, D. A. Synthesis of carbon-supported Pt nanoparticle electrocatalysts using nanocrystalline cellulose as reducing agent. *Green Chem.* **2011**, *13*, 1686−1693.
(19) Shin, Y.; Blackwood, J. M.; Bae, I.-T.; Arey, B. W.; Exarhos, G. J. Synthesis and stabilization of selenium nanoparticles on cellulose nanocrystal. *Mater. Lett.* **2007**, *61*, 4297−4300.
(20) Mahmoud, K. A.; Lam, E.; Hrapovic, S.; Luong, J. H. Preparation of well-dispersed gold/magnetite nanoparticles embedded on cellulose nanocrystals for efficient immobilization of papain enzyme. *ACS Appl. Mater. Interfaces* **2013**, *5*, 4978−4985.
(21) Chen, L.; Berry, R. M.; Tam, K. C. Synthesis of β-cyclodextrin-modified cellulose nanocrystals (CNCs)@ Fe_3O_4@ SiO_2 superparamagnetic nanorods. *ACS Sustainable Chem. Eng.* **2014**, *2*, 951−958.
(22) Lee, I.; Athey, B. D.; Wetzel, A. W.; Meixner, W.; Baker, J. R., Jr. Structural molecular dynamics studies on polyamidoamine dendrimers for a therapeutic application: Effects of pH and generation. *Macromolecules* **2002**, *35*, 4510−4520.
(23) Liu, Y.; Bryantsev, V. S.; Diallo, M. S.; Goddard, W. A., III PAMAM dendrimers undergo pH responsive conformational changes without swelling. *J. Am. Chem. Soc.* **2009**, *131*, 2798−2799.
(24) Hayakawa, K.; Yoshimura, T.; Esumi, K. Preparation of gold-dendrimer nanocomposites by laser irradiation and their catalytic reduction of 4-nitrophenol. *Langmuir* **2003**, *19*, 5517−5521.
(25) Kim, Y. G.; Oh, S. K.; Crooks, R. M. Preparation and characterization of 1−2 nm dendrimer-encapsulated gold nanoparticles having very narrow size distributions. *Chem. Mater.* **2004**, *16*, 167−172.
(26) Esumi, K.; Isono, R.; Yoshimura, T. Preparation of PAMAM-and PPI-metal (silver, platinum, and palladium) nanocomposites and their catalytic activities for reduction of 4-nitrophenol. *Langmuir* **2004**, *20*, 237−243.
(27) Zhao, M.; Crooks, R. M. Dendrimer-encapsulated Pt nanoparticles: Synthesis, characterization, and applications to catalysis. *Adv. Mater.* **1999**, *11*, 217−220.
(28) Jiang, Y.; Gao, Q. Heterogeneous hydrogenation catalyses over recyclable Pd(0) nanoparticle catalysts stabilized by PAMAM-SBA-15 organic-inorganic hybrid composites. *J. Am. Chem. Soc.* **2006**, *128*, 716−717.
(29) Crooks, R. M.; Zhao, M.; Sun, L.; Chechik, V.; Yeung, L. K. Dendrimer-encapsulated metal nanoparticles: Synthesis, characterization, and applications to catalysis. *Acc. Chem. Res.* **2001**, *34*, 181−190.
(30) Rahim, E. H.; Kamounah, F. S.; Frederiksen, J.; Christensen, J. B. Heck reactions catalyzed by PAMAM-dendrimer encapsulated Pd(0) nanoparticles. *Nano Lett.* **2001**, *1*, 499−501.
(31) Ren, N.; Dong, A. G.; Cai, W. B.; Zhang, Y. H.; Yang, W. L.; Huo, S. J.; Chen, Y.; Xie, S. H.; Gao, Z.; Tang, Y. Mesoporous microcapsules with noble metal or noble metal oxide shells and their application in electrocatalysis. *J. Mater. Chem.* **2004**, *14*, 3548−3552.
(32) Esumi, K.; Suzuki, A.; Aihara, N.; Usui, K.; Torigoe, K. Preparation of gold colloids with UV irradiation using dendrimers as stabilizer. *Langmuir* **1998**, *14*, 3157−3159.
(33) Zhang, T.; Wang, W.; Zhang, D.; Zhang, X.; Ma, Y.; Zhou, Y.; Qi, L. Biotemplated synthesis of gold nanoparticle−bacteria cellulose nanofiber nanocomposites and their application in biosensing. *Adv. Funct. Mater.* **2010**, *20*, 1152−1160.
(34) Saito, T.; Isogai, A. TEMPO-mediated oxidation of native cellulose. The effect of oxidation conditions on chemical and crystal structures of the water-insoluble fractions. *Biomacromolecules* **2004**, *5*, 1983−1989.
(35) Sehgal, D.; Vijay, I. K. A method for the high efficiency of water-soluble carbodiimide-mediated amidation. *Anal. Biochem.* **1994**, *218*, 87−91.
(36) Chen, L.; Cao, W.; Grishkewich, N.; Berry, R. M.; Tam, K. C. Synthesis and characterisation of pH-responsive and fluorescent poly(amidoamine) dendrimer-grafted cellulose nanocrystals. *J. Colloid Interface Sci.* **2015**, *450*, 101−108.
(37) Genco, T.; Zemljič, L. F.; Bračič, M.; Stana-Kleinschek, K.; Heinze, T. Characterization of viscose fibers modified with 6-deoxy-6-amino cellulose sulfate. *Cellulose* **2012**, *19*, 2057−2067.
(38) Akhlaghi, S. P.; Berry, R. C.; Tam, K. C. Surface modification of cellulose nanocrystal with chitosan oligosaccharide for drug delivery applications. *Cellulose* **2013**, *20*, 1747−1764.
(39) Tao, L.; Chen, G.; Mantovani, G.; York, S.; Haddleton, D. M. Modification of multi-wall carbon nanotube surfaces with poly-(amidoamine) dendrons: Synthesis and metal templating. *Chem. Commun.* **2006**, *47*, 4949−4951.
(40) Link, S.; El-Sayed, M. A. Spectral properties and relaxation dynamics of surface plasmon electronic oscillations in gold and silver nanodots and nanorods. *J. Phys. Chem. B* **1999**, *103*, 8410−8426.
(41) Panigrahi, S.; Basu, S.; Praharaj, S.; Pande, S.; Jana, S.; Pal, A.; Ghosh, S. K.; Pal, T. Synthesis and size-selective catalysis by supported gold nanoparticles: study on heterogeneous and homogeneous catalytic process. *J. Phys. Chem. C* **2007**, *111*, 4596−4605.
(42) Li, J.; Liu, C. Y.; Liu, Y. Au/graphene hydrogel: Synthesis, characterization and its use for catalytic reduction of 4-nitrophenol. *J. Mater. Chem.* **2012**, *22*, 8426−8430.

DOI: 10.1021/acssuschemeng.5b00110
ACS Sustainable Chem. Eng. 2015, 3, 978−985